7 Tesla magnetic resonance spectroscopy estimates of GABA concentration relate to physiological measures of tonic inhibition in the human motor cortex

Ilenia Paparella[1] , Paolo Cardone[2] , Benedetta Zanichelli[1], Laurent Lamalle[1] , Fabienne Collette[1] , Siya Sherif[1] , Mikhail Zubkov[1] , William T. Clarke[3] , Charlotte J. Stagg[3,4] , Pierre Maquet[1,5] and Gilles Vandewalle[1]

[1]*GIGA-Research, CRC-Human Imaging Unit, 8 allée du Six Août, Batiment B30, University of Liège, Liège, Belgium*

[2]*GIGA-Research, Coma Science Group, GIGA-Consciousness, University of Liège, Liège, Belgium*
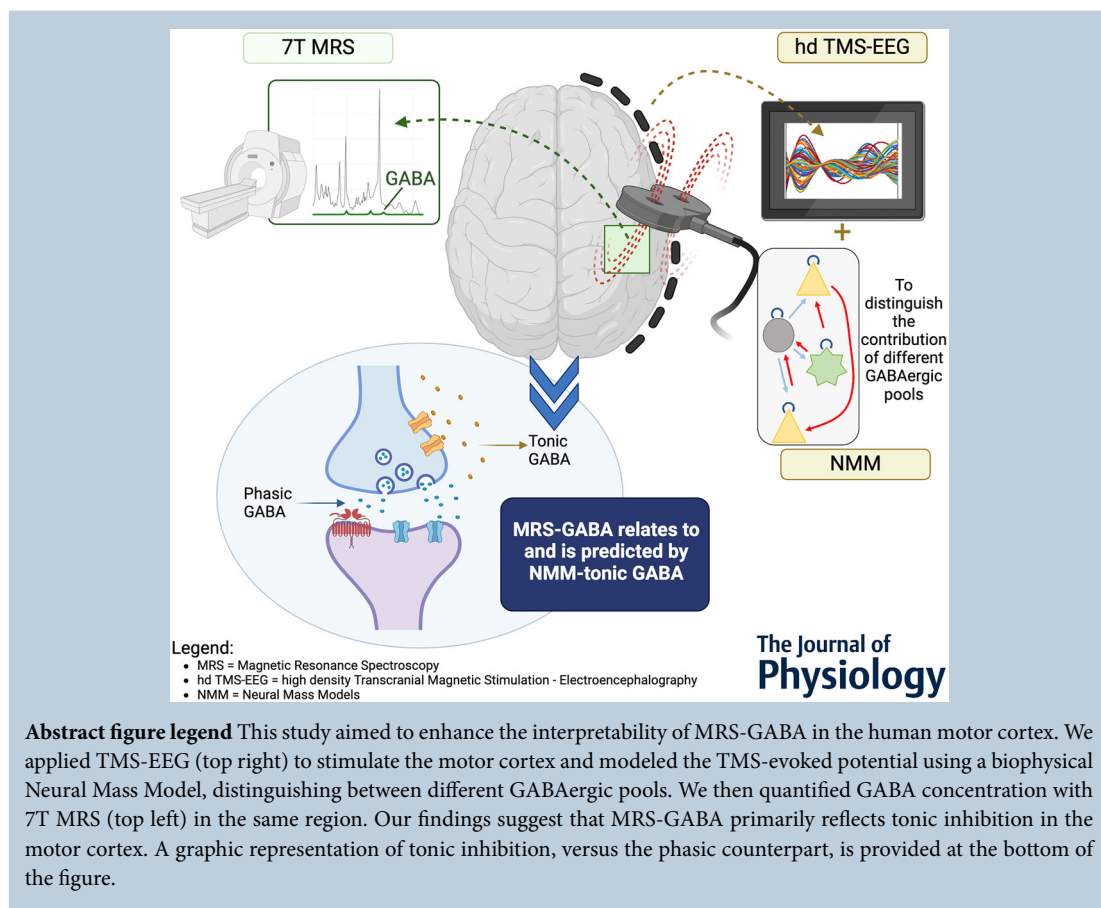
[3]*Wellcome Centre for Integrative Neuroimaging, FMRIB, Nuffield Department of Clinical Neurosciences, University of Oxford, Oxford, UK*

[4]*Medical Research Council Brain Network Dynamics Unit, University of Oxford, Oxford, UK*

[5]*Department of Neurology, Domaine Universitaire du Sart Tilman, CHU de Liège, Belgium*

Handling Editors: Richard Carson & James Coxon

The peer review history is available in the Supporting Information section of this article (https://doi.org/10.1113/JP287311#support-information-section).

Abstract figure legend This study aimed to enhance the interpretability of MRS-GABA in the human motor cortex. We applied TMS-EEG (top right) to stimulate the motor cortex and modeled the TMS-evoked potential using a biophysical Neural Mass Model, distinguishing between different GABAergic pools. We then quantified GABA concentration with 7T MRS (top left) in the same region. Our findings suggest that MRS-GABA primarily reflects tonic inhibition in the motor cortex. A graphic representation of tonic inhibition, versus the phasic counterpart, is provided at the bottom of the figure.

Abstract GABAergic neurotransmission within the cortex plays a key role in learning and is altered in several brain diseases. Quantification of bulk GABA in the human brain is typically obtained by magnetic resonance spectroscopy (MRS). However, the interpretation of MRS-GABA is still debated. A recent mathematical simulation contends that MRS detects extrasynaptic GABA, mediating tonic inhibition. Nevertheless, no empirical data have yet confirmed this hypothesis. Here we collected ultra-high-field 7 Tesla MRS and transcranial magnetic stimulation coupled with high-density electroencephalography (TMS-hdEEG) from the motor cortex of 20 healthy participants (age 23.95 ± 6.4 years), while they were at rest. We first applied a neural mass model (NMM) to TMS-evoked potentials to disentangle the contribution of different GABAergic pools. We then assessed to which of these different pools MRS-GABA was related to by means of parametric empirical Bayesian (PEB) analysis. We found that MRS-GABA was mostly positively related to the NMM-derived measures of tonic inhibition and overall functionality of the GABAergic synapse. This relationship was reliable enough to predict MRS-GABA from NMM-GABA. These findings clarify the mesoscopic underpinnings of GABA levels measured by MRS. Our work will help fulfil the promises of MRS-GABA, enhancing our understanding of human behaviour, brain physiology and pathophysiology.

Corresponding authors Ilenia Paparella and Gilles Vandewalle: GIGA-CRC-Human Imaging, Bâtiment B30, 8 Allée du Six Août, University of Liège-Sart Tilman, 4000 Liège, Belgium.   Email: ipaparella@uliege.be, gilles.vandewalle@uliege.be

Key points

- GABA neurotransmission is essential for synaptic plasticity and learning (especially motor learning) and is altered in several brain disorders, such as epilepsy and stroke.
- Quantification of GABA in the human brain is typically obtained by magnetic resonance spectroscopy (MRS). However, the interpretation of MRS-GABA is still debated.
- By using a biophysical neural mass model, here we show that MRS-GABA relates to physiological measures of tonic inhibition in the human cortex.

Introduction

GABA plays a crucial role in maintaining the excitation/inhibition balance in the brain, which is pivotal for optimal brain functioning (Le Roux et al., 2008). GABA neurotransmission is essential for synaptic plasticity (Stagg et al., 2011a) and learning (especially motor learning; Bachtiar et al., 2015; Kolasinski et al., 2019; Stagg et al., 2014) and is altered in several brain disorders, such as epilepsy and stroke (Paparella et al., 2023). Despite its functional significance, the interpretation of non-invasive GABA measurements in humans are challenged by the complexity of GABA signalling. After its release in the synaptic cleft, GABA binds with two major postsynaptic receptors, $GABA_A$ and $GABA_B$. GABA receptors are widely expressed in the CNS and account for $\sim$20% of the synapses in the cerebral cortex, hippocampus, thalamus and cerebellum (W. Zhang et al., 2021). GABA is also found in the extracellular space where it binds to extrasynaptic $GABA_A$ receptors

Ilenia Paparella is a PhD candidate in Biomedical and Pharmaceutical Sciences from the University of Liège (Belgium), working on a multimodal approach combining neuroimaging (magnetic resonance spectroscopy) and electrophysiology (transcranial magnetic stimulation combined with high-density electroencephalography) to find new biomarkers of stroke recovery. Her aim is to find neural signatures in acute patients that predict good motor recovery and prognosis.

(Belelli et al., 2009). These two different GABA pools play different roles in the brain with synaptic GABA triggering phasic inhibition and extracellular GABA mediating tonic inhibition (Stagg et al., 2011b), which regulates neuronal gain and causes lasting modifications of neuronal activity, such as during learning.

Several techniques are available in humans to non-invasively probe specific aspects of GABA dynamics, ranging from molecular imaging (magnetic resonance spectroscopy, MRS; positron emission tomography, PET) to electrophysiology (electroencephalography, EEG) and brain stimulation (transcranial magnetic stimulation, TMS). None of these techniques accounts, alone, for all aspects of GABAergic signalling, making it therefore challenging to fully establish the contribution of phasic and tonic inhibition in human cognition. MRS allows for repeated, quantitative measurements of local GABA concentration without requiring invasive radio tracers (unlike PET) or a measurable motor output (unlike TMS), resulting in an enhanced clinical translatability. MRS is particularly promising when carried out at ultra-high-field magnetic resonance imaging (MRI) ($\geq$7 Tesla, T), given the improved signal-to-noise-ratio and resolution compared to lower fields. Nevertheless, MRS-GABA cannot capture the dynamics of different GABAergic pools. A recent mathematical simulation suggested that MRS is probably reflects free extracellular GABA (Lea-Carnall et al., 2023) and could therefore provide a measure of tonic inhibition. However, this hypothesis is not yet supported by empirical data. Clarifying what is being measured by MRS would improve our understanding of MRS-GABA changes in behaviour and in neurological disorders, ultimately opening avenues for innovative care and treatment option for patients.

Here, we used a neural mass model (NMM) (Moran et al., 2013) of TMS-evoked brain potentials recorded with high-density EEG (Adams et al., 2021a), to model the dynamics of different GABAergic pools in a neuronal population of the motor cortex of 20 healthy subjects. We chose the motor cortex as motor evoked responses can be used as an objective means to standardize intensity and functional location of the TMS hotspot across participants and given GABA relevance for motor learning. NMM estimation of GABA activity has been validated by pharmacological interventions in humans and is considered equivalent to invasive interventions in animals (Moran, Jung, et al., 2011; Moran, Symmonds, et al., 2011; Muthukumaraswamy et al., 2013, 2015). We further collected ultra-high field 7 T-MRS data over the same cortical area in the same healthy participants. We aimed to test whether MRS-GABA was associated with NMMs' estimation of tonic/phasic inhibition, with the hypothesis that GABA concentration would be related to physiological measures of tonic inhibition.

Materials and methods

Participants

The study conformed to the standards set by the latest revision of the *Declaration of Helsinki*, except for registration in a database, and the procedures were approved by the Ethical Committee of the CHU and Faculty of Medicine of Liège (ethical approval number: B707202042974). Participants gave their written informed consent prior to their enrolment and received financial compensation for their participation. Exclusion criteria were as follows: body mass index >25 kg/m^2; smoking or excessive alcohol consumers (>14 units/week) or other addiction; use of sedative drugs, Na or Ca channel blockers, or other drugs acting on GABA/glutamate; metal inside the body, recent psychiatric history, severe head trauma or sleep disorders, chronic medications; be left-handed. Twenty female participants were recruited (23.95 ± 6.44 years). Whether sex affects GABA concentration is still debated (Epperson et al., 2002). Some studies report contradictory sex differences in GABA (possibly due to regional variation) (O'Gorman et al., 2011; Sanacora et al., 1999), whereas other studies report no differences at all (Chang et al., 2009), particularly in the motor cortex (Pandya et al., 2019). We decided to recruit only women to avoid potential sex biases and because mostly women responded to our initial call for participants. The hormonal phase of our participants was collected and accounted in our analysis when relevant. A strong bias arising from hormonal phase is unlikely in our within-subjects design, given that TMS-EEG and MRS were collected on the same day or on consecutive days. Wake-up time and sleep duration/quality were also collected to avoid sleep deprivation from altering our results (see Experimental protocol). Table 1 shows all detailed participant demographics.

Experimental protocol

Testing times were kept constant across participants to account for potential circadian variations in GABAergic activity (Chellappa et al., 2016) (Fig. 1). All participants came to the laboratory at 08.00 h. They were asked not to consume caffeine or alcohol containing beverages for >24 h prior to their admission. They were asked to follow their normal sleep schedule the night before the study. Participants underwent a 30 min structural scan at 7 T MRI, which was later used for the TMS neuronavigation session and EEG source reconstruction. At around 09.00 h participants started the TMS-EEG session, which lasted for about 3 h. After a small lunch break (caffeine/alcohol free), most participants (14) underwent an MRS session (at ~15.00 h), which lasted around 1 h. The voxel of interest (green box, Fig. 1) was positioned over the same area

Table 1. Participants' demographics

	Sample ($N = 20$)
Age (years)	23.95 ± 6.44
Sex	Female
BMI (kg/m^2)	23.95 ± 3.87
Hormonal phase	40% menstruation
	30% follicular phase
	25% luteal phase
	5% no period due to contraceptive pill
Handedness	Right
Wake-up time	6 h 32 min $\pm$ 20 min
Sleep duration	6 h 44 min $\pm$ 1 h

Characteristics of the total study sample. BMI: body mass index. The hormonal phase is computed as the number of days from the start of the last menstrual cycle before participating in the study. Participants were also asked to communicate the start of the following menstrual cycle to take the length of their cycle into account. Wake-up time and scores of sleep duration/quality are as reported in the self-completion Leeds Sleep Evaluation Questionnaire (Parrott & Hindmarch, 1978). Values are provided as average $\pm$ standard deviation (SD).

previously stimulated with TMS-EEG by using anatomical landmarks. The remaining (six) participants decided to have the MRS on the following days (at 15.00 h) in which case the sleep requirement and questionnaire were

repeated. For these participants we further ensured that the MRS session was kept at the same hormonal phase.

Data acquisition

Structural T1 scan

A T1-weighted structural image was acquired using a 7 T MRI system (Terra, Siemens Healthineers, Erlangen, Germany) with a 32-channel receiver and one-channel transmit head coil (Nova Medical, Wilmington, MA, USA). Structural MRI data were acquired with a Magnetization Prepared Rapid Acquisition Gradient Echo (MPRAGE) sequence: TR, 2300 ms; TE, 2.76 ms; slice thickness, 1.0 mm; in-plane resolution 1.0×1.0 mm^2, GRAPPA factor = 2. The acquired structural image was used to inform the neuronavigation during the TMS-EEG session.

TMS-EEG

TMS-EEG data were recorded with a 60-channel TMS-compatible EEG amplifier (Eximia EEG, Nexstim, Helsinki, Finland), and TMS was delivered by means of a Focal Bipulse 8-Coil (Eximia TMS) combined with a magnetic resonance-guided navigation system (eXimia NBS). The EEG amplifier gates the TMS artefact and prevents saturation by means of a proprietary
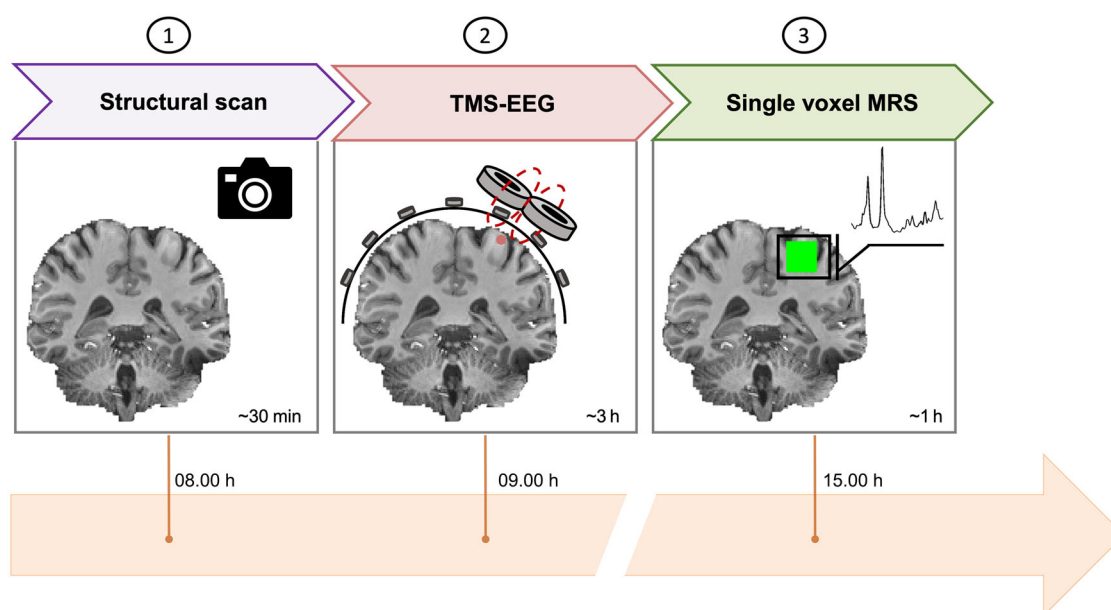
Figure 1. Graphical representation of the experimental protocol
All participants arrived at the lab at 08.00 h. They first underwent a 30 min structural scan at 7 T MRI. At 09.00 h, the TMS-EEG started. Our stimulation spot (here as a red dot) was in the left motor cortex and was located on the structural scan. The TMS-EEG session lasted around 3 h. Afterwards, participants underwent an MRS session at 7 T MRI (roughly at 15.00 h). The voxel of interest (here represented as a green box) was positioned over the same area previously stimulated with TMS-EEG by using anatomical landmarks. The MRS session lasted around 1 h. An example cropped spectrum is also provided.

sample-and-hold circuit that ensures the absence of TMS-induced magnetic artefacts from 8 ms after TMS.

Our stimulation site was the right motor hotspot for the first dorsal interosseous (FDI) on the left hemisphere, defined as the scalp location where the largest and most consistent motor-evoked potentials could be identified in the FDI. The TMS coil orientation was then adjusted to obtain an artifact-free TMS-evoked potential (TEP) following recent recommendations (Hernandez-Pavon et al., 2023). Resting motor threshold was defined as the minimum intensity needed to elicit a peak-to-peak motor-evoked response with an amplitude of more than 50 µV in at least 5 out of 10 subsequent trials while the targeted muscle was at rest.

The stimulation session consisted of 250 pulses at a stimulation intensity below resting motor threshold to reduce muscular contamination in the EEG (Fecchio et al., 2017). Electromyography (Nexstim EMG) was recorded via disposable ECG electrodes placed over the FDI of the right hand, using a belly-tendon montage with a ground electrode over the ulnar styloid process. During the session, participants were seated on a comfortable reclining bed, with their eyes open and their right hand positioned on a pillow placed over their lap. They were instructed to fixate a black dot placed on the wall in front of them at eye level and to keep the targeted muscle relaxed while EMG was continuously monitored on a computer screen. The inter-stimulus interval (ISI) was randomly set to 1900–2200 ms.

EEG signal was band-pass filtered between 0.1 and 500 Hz and sampled at 1450 Hz. All electrode impedances were maintained $<5\,k\Omega$. Electro-oculogram was recorded with two additional bipolar electrodes. During the EEG recording, participants' perception of the clicks produced by the TMS coil discharge was eliminated using earplugs continuously playing a pink masking noise (<90 dB, adjusted per participant prior to each recording). Bone conduction was minimized by applying a thin foam layer between the EEG cap and the TMS coil. The absence of an auditory evoked response was verified during each recording and was confirmed by delivering, in a short sham session, 30–40 pulses parallel to the scalp while the masking noise was played at the same level. At the end of each recording, electrode positions on the participants' head were recorded. Participants were continuously monitored by a member of the team to ensure they did not fall asleep or doze off during the session.

MRS

MRS data were acquired with the same 7 T MRI system. Participants were instructed to lay still at rest while in the MRI scanner without falling asleep. Dielectric pads (Multiwave Imaging, Marseille, France) were placed over the left central sulcus to increase B1 efficiency over the M1 voxel of interest (VOI). B1 efficiency was imaged using actual flip angle imaging (AFI): field of view 240×240 mm^2, repetition times (TR1/2) 6 / 30 ms, Echo Time (TE) 2.58 ms; non-selective flip angle 60°; slice thickness 2.5 mm, in-plane resolution. To enable the placement of the MRS voxel, we repeated the T1 structural acquisition as detailed above. Coronal and axial images were resampled from the sagittal T1-weighted image and used to place a $2 \times 2 \times 2$ cm^3 VOI. Anatomical landmarks from the screenshot of the motor hotspot stimulated in the previous TMS-EEG session were used to guide voxel positioning over the T1 image. Given the voxel size, we cannot exclude that in some cases the VOI also included parts of the sensory cortex. Figure 2 provides a heatmap of the VOI and TMS-EEG spot across all participants. Shimming was performed in two steps: first using the vendor's own GRE shimming and second using FASTMAP (Gruetter & Tkáč, 2000). MRS data were acquired using a semi-LASER sequence (localization by adiabatic selective refocusing) provided as part of the Center for Magnetic Resonance Research, University of Minnesota Spectroscopy package SEMI-LASER (MRM 2011, NMB 2019) Release 2016-12, https://doi.org/10.1002/nbm.4218: TR = 5000 ms, TE = 26 ms (TE1/2/3 = 7 ms, 10 ms, 9 ms), $20 \times 20 \times 20$ mm^3 voxel, 64 averages per block, TA = 5 min 20 s, using per-subject calibrated VAPOR (Variable Power RF pulses with Optimized Relaxation delays) water suppression. A standardized description of MRS hardware, data acquisition, analysis and quality assessment, in line with recent guidelines (Lin et al., 2021), is provided in Table 2.

Data analysis

TMS-EEG and NMM

TMS-EEG data were preprocessed with Statistical Parametric Mapping 12 (SPM12, http://www.fil.ion.ucl.ac.uk/spm/) and analysed with MATLAB R2019 (MathWorks, Natick, MA, USA). Data were visually inspected to reject artifacted channels and trials (blink, body movements, slow eye movements and other artifacts; rejection rate of around 10%). EEG signals were re-referenced to the average of all good channels. Continuous EEG recordings were lowpass-filtered at 80 Hz, down-sampled from 1450 to 1000 Hz and then highpass-filtered at 1 Hz. Individual trials were then epoched between -100 before and 300 ms after TMS pulses. Baseline correction (-100 and -1.5 ms before TMS pulses) was applied. Robust averaging was used to compute the mean evoked response.

We then used NMM (see Moran et al., 2013 for full details of the model, including a mathematical equation), within the Dynamic Causal Modelling (DCM) (Friston et al., 2003) framework, to model our evoked response. NMMs, originally used to study multi-region network responses, are applied increasingly to describe molecular factors underlying brain activity in a single region. NMM models event-related potentials as the response of a network to exogenous inputs, by inferring neuronal states within a given cortical area comprising four subpopulations of neurons, namely deep and superficial pyramidal cells, excitatory stellate cells, and inhibitory interneurons. These sub-populations exhibit self-inhibition controlling neuronal gain and communicate through excitatory and inhibitory connections (Moran et al., 2013). The model also includes active currents that describe ligand-gated excitatory and inhibitory ion flow, mediated through glutamatergic (AMPA and NMDA) and GABAergic (GABA$_A$) receptors (Moran, Symmonds, et al., 2011). GABA$_A$, AMPA and NMDA measures are the rate constant of the receptors lumped over the entire circuit. A graphical representation of the NMM is provided in Fig. 3*A*. Model accuracy was checked by computing the Pearson's correlations between observed and modelled data and R^2 values, over the first three Modes of the model (Fig. 3*C*, *D*).

Importantly, this model allows for the distinction between tonic background inhibition, mediated by cell inhibitory self-connections, and phasic inhibition, modelled by the projections from interneurons to the other cells (Adams et al., 2021b).

The TMS pulse is assumed to represent the input as would be typically induced by sensory stimuli. To estimate which NMM parameter (and how) contributes to the evoked response, DCM uses generative or forward models for evoked EEG responses and fits these models using a variational Bayesian inversion scheme. We modelled the active source (individual MRI coordinates of the TMS hotspot) by means of a single equivalent current dipole (ECD) within an electromagnetic forward model over the 5–50 ms TEP, a time window where changes in EEG can arguably be attributed to the sole local effects of the TMS. This model used a 'boundary element method' approach, with homogeneously and isotropically conductive volumes delimited by the brain, cerebrospinal fluid (CSF), skull and scalp surfaces. Individual head models are derived using an inverse spatial normalization of a canonical mesh for each participant (MRI T1-sequence, 20,400 dipoles). The position of the 60 electrodes was coregistered in each participant before forward model computation. A lead-field mapping of cortical sources onto measured signals was parameterized for orientation and location of the ECD. In the NMM we used, all the parameters were allowed to vary, to enable the model to recreate complex neurophysiological brain states. An example of observed and modelled brain response (averaged over 250 TMS pulses) is provided in Fig. 3*B*.
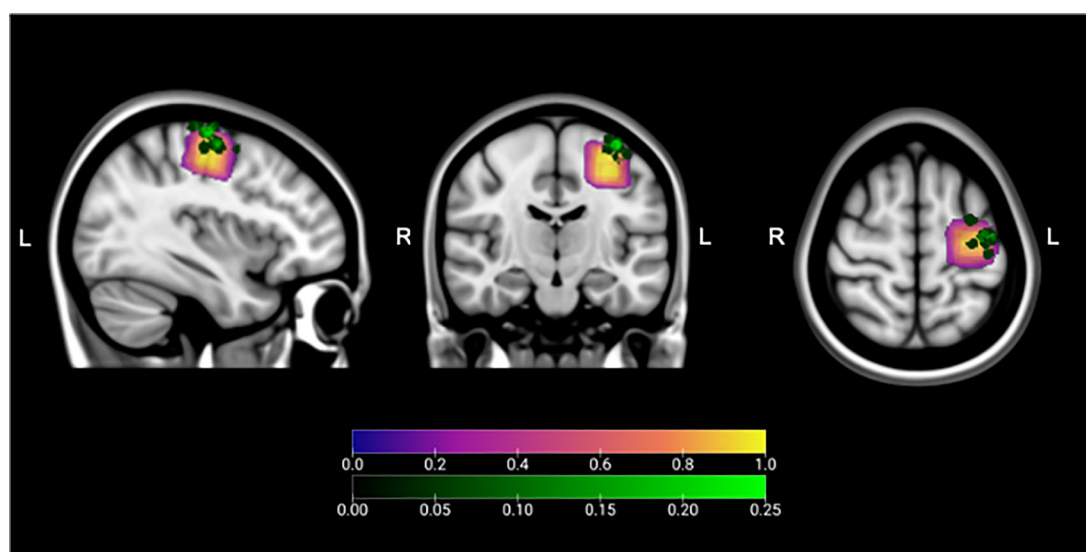

Figure 2. Probabilistic heatmap of MRS VOI placement and TMS-EEG hotspot location across participants
The heatmaps are shown on the sagittal, coronal and axial view of the MNI_152_T1_1mm template (coordinates [−37, −16, 61]) provided by FSL (Jenkinson et al., 2012). The colour scales represent the proportion of participants whose VOI (upper) or TMS-EEG spot (lower) overlapped in that voxel. As a rule, each VOI was placed in the left primary motor cortex, as close as possible to the TMS-EEG spot (by following anatomical landmarks), and avoiding non-brain tissue (e.g. the dura) that could induce artifacts in the MRS signal.

Table 2. MRSinMRS checklist for a 7 T MRS study

1. Hardware	
a. Field strength	7 T
b. Manufacturer	Siemens Healthineers, Erlangen, Germany
c. Model (software version if available)	Magnetom Terra 7T (VE12U-SP01)
d. RF coils: nuclei (transmit/receive), number of channels, type, body part	32-channel receiver and one-channel transmit head coil (Nova Medical, Wilmington, MA, USA)
e. Additional hardware	–
2. Acquisition	
a. Pulse sequence	Semi-LASER
b. Volume of interest and VOI locations	Single voxel placed over the hand knob located in the motor cortex
c. Nominal VOI size [cm^3, mm^3]	Anatomy-matched, $2 \times 2 \times 2$ cm^3
d. Repetition time (TR), echo time (TE) [ms, s]	TR = 5000 ms, TE = 26 ms (TE1/2/3 = 7 ms, 10 ms, 9 ms)
e. Total number of excitations or acquisitions per spectrum (NA)	120
f. Additional sequence parameters (spectral width in Hz, number of spectral points, frequency offsets)	Spectral width: 6000 Hz FID points: 2048 Excitation offset: -2.0 ppm
g. Water suppression method	Per-subject calibrated VAPOR (Variable Power RF pulses with Optimized Relaxation delays) water suppression
h. Shimming method, reference peak and thresholds for 'acceptance of shim' chosen	Shimming was performed in two steps: first using the vendor's own GRE shimming, and second using FASTMAP (Gruetter & Tkáč, 2000).
i. Triggering or motion correction method (respiratory, peripheral, cardiac triggering, incl. device used and delays)	None
3. Data analysis methods and outputs	
a. Analysis software	Both processing and fitting was done in FSL-MRS (Clarke et al., 2021)
b. Processing steps deviating from quoted reference or product analysis software (vendor, version)	None
c. Output measure (e.g. absolute concentration, institutional units, ratio) processing steps deviating from quoted reference or product	Ratio to total creatine (tCr, Cr + PCr).
d. Quantification references and assumptions, fitting model assumptions	GABA was quantified as referenced to total creatine
5. Data quality	
a. Reported variables (SNR, linewidth – with reference peaks)	SNR, FWHM
b. Data exclusion criteria	The exclusion criteria for the data were as follows: visible artifacts (none detected), water linewidths at full width at half maximum (FWHM) >15 Hz or low signal/noise ratio (SNR)
c. Quality measures of post-processing model fitting (e.g. CRLB, goodness of fit, SD of residual)	%CRLB
d. Sample spectrum	Fig. 4*A*

MRS

Quantitative analyses of the spectra were performed using the open source FSL-MRS (Clarke et al., 2021) analysis toolbox. Raw ('twix'/''.dat') MRS data were first converted into the standard data format for MRS (NIfTI-MRS) using the conversion program *spec2nii* (Clarke et al., 2022). Converted data were then pre-processed with *fsl_mrs_preproc*, the pre-packaged processing pipeline for non-edited single voxel MRS data provided by FSL-MRS. The pipeline performs all the processing operations recommended in the community-driven consensus paper (Near et al., 2021), including coil combination, phase and frequency alignment of individual transients, averaging, eddy current correction, removal of residual water with HLSVD (Hankel-Lanczos singular value decomposition),
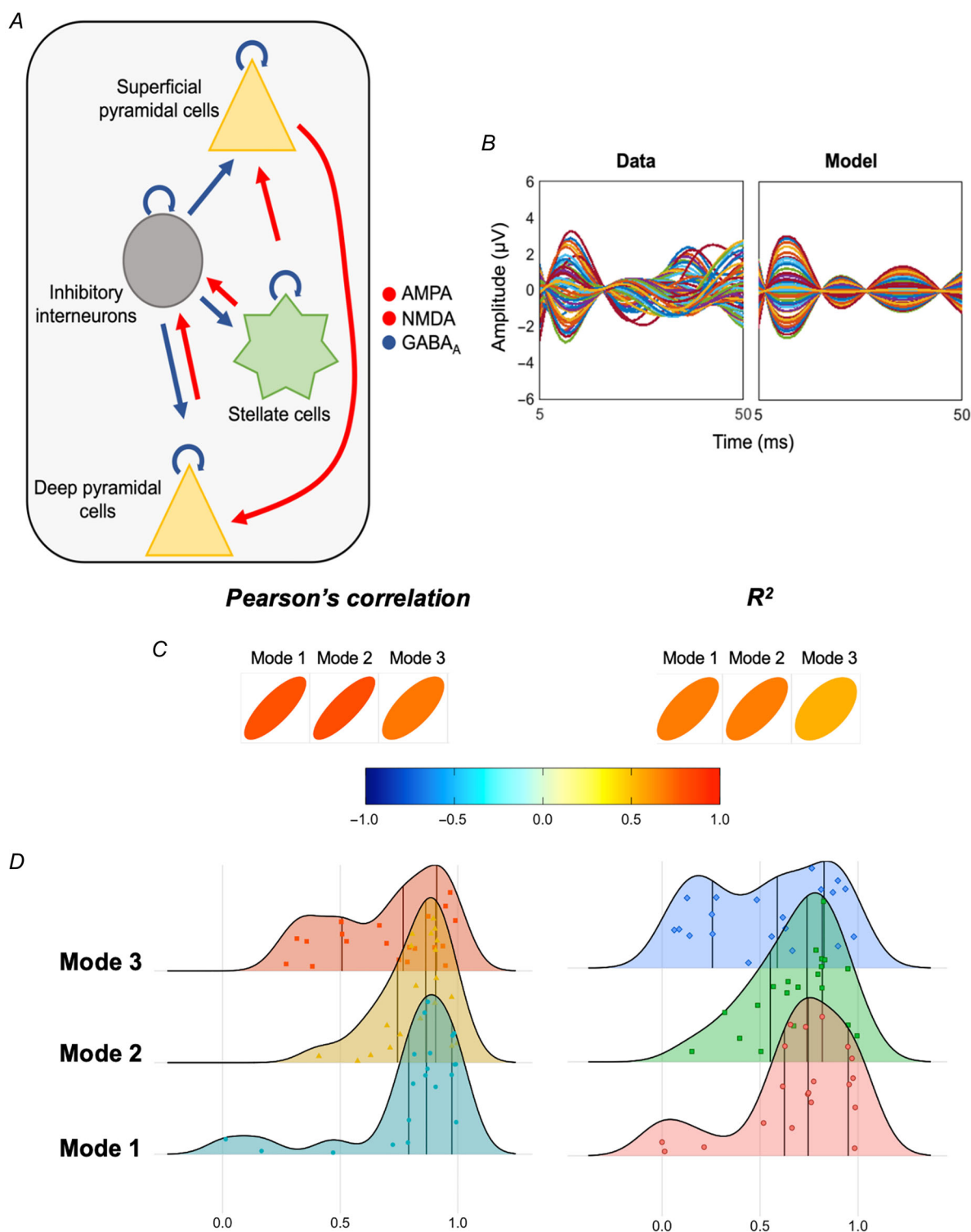
Figure 3. Neural mass model, example of model fit and model accuracy

A, NMM decomposes a cortical area into four neuronal subpopulations: superficial and deep pyramidal cells (yellow), spiny stellate cells (green) and inhibitory interneurons (grey). Each subpopulation is assigned to a particular cortical layer and projects to the other subpopulations via anatomically plausible excitatory (red) and inhibitory (blue arrows) connections and have inhibitory feedback-loops controlling neuronal gain. NMM also provides information on the density and the activity of three mains receptors: AMPA and NMDA (red) mediating excitatory connections and $GABA_A$ mediating inhibitory ones (blue). This figure was simplified from Paparella et al. (2023). *B*, example

of model fit with an observed (left) and modelled (right) TMS-evoked response, averaged over 250 TMS pulses, for one of our participants. The response is plotted as a function of time and amplitude. Each line represents a channel. *C*, graphical representation (top) of the Pearson's correlation between observed and plotted data (left) and R^2 values (right), across the first three Modes of the model. *D*, density plots (bottom) making up the values in *C*, showing individual data (single dots) and interquartiles (black bands).

and zero-order phase correction. *Fsl_mrs_sim* was used to create a set of basis spectra by providing precise description of the sLASER sequence (timings, RF pulses and relevant gradients). An empirically measured macromolecular baseline was added to the basis set. The generated basis spectra were then fitted to the data using a Markov chain Monte Carlo (MCMC) optimization. To quantify the proportion of white matter, grey matter and CSF in the VOI, the *svs_segment* command was applied to the T1 image, previously preprocessed using the fsl_anat structural processing pipeline in the FMRIB software library (FSL) (Jenkinson et al., 2012), which performs some pre-processing steps including bias correction, brain extraction (Smith, 2002), registration to standard space (Jenkinson & Smith, 2001) and tissue segmentation (Y. Zhang et al., 2001). All the metabolites were corrected for the proportion of total brain tissue in the VOI. There was no strong correlation ($>\pm0.3$) between GABA and other metabolites, indicating good spectral separation was achieved. The exclusion criteria for the data were as follows: visible artifacts (none detected), water linewidths at full width at half maximum (FWHM) >15 Hz or low signal/noise ratio (SNR) (Juchem et al., 2021). The quality check was performed through the *fsl_mrs_summarise* command. None of the data met the exclusion criteria, and thus all were included for further analysis. GABA concentration is expressed as a ratio of total creatine (tCr – validated reference compound in GABA MRS; Mullins et al., 2014) and reported as MRS-GABA. A summary of the analysis steps is included in Table 2. Figure 4 provides examples of good, average and bad quality data both raw and fitted (Fig. 4*A*), as well as MRS quality control metrics (Fig. 4*B–D*) and a typical MRS spectrum and fit quality including GABA and macromolecule fit estimates (Fig. 4*E*).

Statistics

NMMs describe the average microscopic activity of the neural subpopulations within a cortical column in the region of interest. The first-level analysis infers neural responses of individual TMS-EEG data by inverting the Bayesian model (Moran et al., 2007; Zeidman, Jafarian, Corbin, et al., 2019), which allows finding the parameters that offer the best trade-off between predictions and observations. Briefly, the NMM estimates: the connectivity among the four subpopulations of neurons (stellate, superficial and deep pyramidal cells and inhibitory interneurons) as well as their respective inhibitory feedback-loops; the membrane threshold lumped across all subpopulations; GABA$_A$, AMPA and NMDA receptor density; the mean field of all subpopulations; the background activity; and the voltage-gated channel capacitance (Cl$^-$, Na^{2+}, Ca^{2+}, K$^-$). These results are stored in the H, MT, T, S, E and CV matrix, respectively. Once we estimated the NMM for each subject, we then tested whether MRS-GABA was related to any of the parameters in our model using parametrical empirical Bayes (PEB) (Zeidman, Jafarian, Seghier, et al., 2019) as included in SPM12. To avoid dilution of evidence, we reduced the search space (Zeidman, Jafarian, Seghier, et al., 2019) by carrying out a PEB analysis only over the T and H matrix of the NMM. These two matrices were selected as they are the only parameters in the NMM providing GABAergic information both in isolation and in interaction with the glutamatergic counterpart. In PEB, the probability densities of all parameters of the NMM are collated and modelled at the second level with any unexplained between-subject variability captured by a covariance component mode. PEB then performs Bayesian model reduction (BMR), which 'prunes' any parameter not contributing to the model evidence by automatically searching over reduced models (those with some parameters switched off). Then, Bayesian model average (BMA) is calculated over the models from the final iteration of the greedy search. Only NMM parameters with a strong significant relationship with MRS-GABA, as indexed by a posterior probability (Pp) >0.99, are reported in the Results. To provide visual representation of our results, individual peak estimates were extracted to obtain linear regression plots. We then used leave-one-out (LOO) to test the meaningfulness of the relationship (predictive validity) found between MRS- and NMM-GABA. A PEB model was fitted to all but one subject, and covariates for the left-out subject were predicted. This was repeated with each subject left out and the accuracy of the prediction was recorded. A bias arising from hormonal phase is unlikely in our within-subjects design, given we ensured participants kept the same hormonal phase when their TMS-EEG and MRS measures were collected. However, to further ensure our associations were not influenced by participants' hormonal phase, the LOO analysis was repeated accounting for percentage of menstrual cycle. This value was taken as a proxy of progesterone levels given its known link with GABA (Gilfarb & Leuner, 2022; Maguire et al., 2005), and was computed as (day from cycle start/cycle length) $\times 100$.
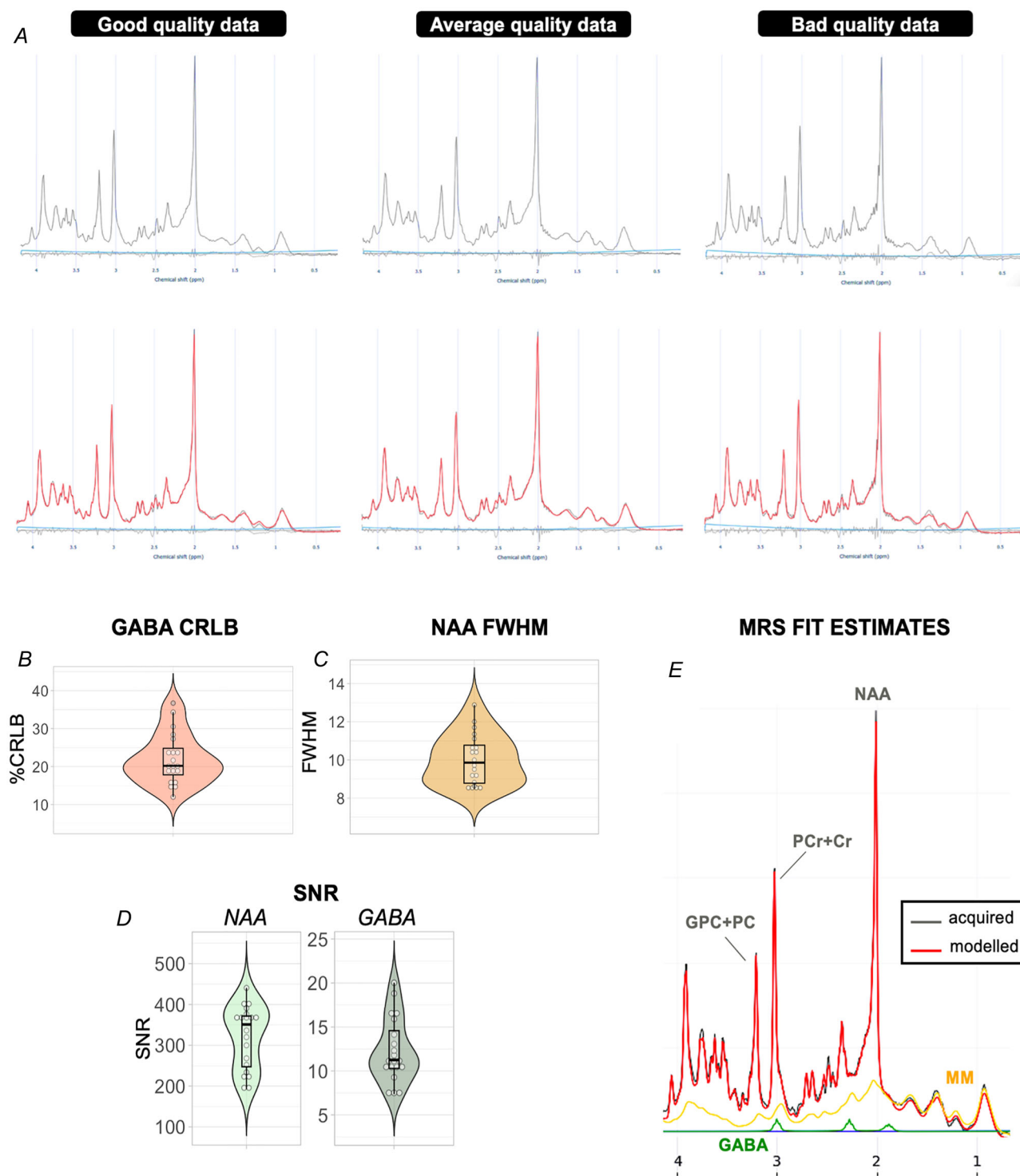
Figure 4. Representative spectra, MRS QC metrics and typical fit quality
A, representative spectra from the hand knob (motor cortex) acquired on a 7 T scanner. Both raw (upper row) and fitted data (lower row) are shown. From left to right, good, average and bad data quality spectra are shown, respectively. The chemical shift axis is labelled in ppm units. *B–D*, violin plots showing three MRS QC metrics: GABA %Cramér–Rao lower bound (*B*, CRLB), NAA full width at half maximum (*C*, FWHM), and NAA and GABA SNRs (*D*). Individual values are indicated as white dots, as well as summary statistics as box plots. *E*, a typical MRS spectrum (in grey) and fit quality (in red), including baseline (in blue), GABA (in green) and macromolecules (in yellow) fit estimates.

Optimal sensitivity and power analysis in DCM/PEB remains under investigation. We nevertheless computed a prior sensitivity analysis to get an indicator of the minimum detectable effect size in our main analyses given our sample size. According to G*Power 3 (version 3.1.9.4) (Erdfelder et al., 2009) taking into account a power of 0.8 and an error rate of 0.05, a sample size of 20 allowed us to detect a medium effect size $r > 0.27$ (confidence interval: -0.2, 0.64; $R^2 > 0.07$, R^2 confidence interval: 0.04–0.41) within a linear multiple regression framework including one predictor. Based on this, we deemed the sensitivity reasonable.

Results

The PEB analysis revealed that MRS-GABA correlated positively with the self-inhibitory feedback loop of almost all the subpopulation of cells included in the model, namely the inhibitory interneurons, stellate and deep pyramidal cells (Fig. 5*A*). PEB further showed that MRS-GABA was negatively related with the excitatory connection from stellate to superficial pyramidal cells and to the inhibitory connection from inhibitory interneurons to deep pyramidal cells. At the receptor level, the only significant effect was a positive relationship with the activity of $GABA_A$. The effect sizes of each significant relationship are reported in Fig. 5*A* and represent the rate of change of the NMM parameter as a function of MRS-GABA, with the sign specifying the direction of the relationship. As an example, the effect size of the relationship between MRS-GABA and the self-inhibitory feedback loop of the inhibitory interneuron is 5.15, meaning that when MRS-GABA increases onefold, the inhibition of the inhibitory interneurons increases as well by 5.15 times (in the units of the underlying DCM). Figure 5 includes two linear regression plots to represent the positive relationship found between MRS-GABA and NMM-tonic inhibition (calculated as the mean of the significant self-inhibitory feedback loops' peak estimates) (Fig. 5*B*) and between MRS-GABA and the NMM-$GABA_A$ receptor activity (Fig. 5*C*). These plots are for display purposes only and do not substitute for the outcomes of the PEB analysis. Menstrual cycle phase was also represented by colour-coding data points according to cycle phase categories.

We then wanted to further assess whether the size of the positive relationship between NMM-tonic inhibition and MRS-GABA was meaningful enough that we could predict one with the other. Assessing predictive validity is particularly important for studies determining the clinical significance of model parameters. Several NMM parameters showed a significant relationship with MRS-GABA, and we could not use them all for the predictive analysis, especially given our small sample size. We used the NMM parameter encoding for the self-inhibitory feedback loop of the inhibitory interneurons (NMM-self_II) for our next analysis as it constitutes the most canonical proxy of tonic inhibitory activity within the NMM. We then used LOO to test if we could predict MRS-GABA from NMM-self_II. The out-of-samples correlation of the actual MRS-GABA over the (expected value of) predicted MRS-GABA for each left-out subject was significant (Pearsons's rho $= 0.39$, $P = 0.04$) (Fig. 5*D*). Therefore, the relationship between NMM-self_II (a marker of tonic inhibition) and MRS-GABA was sufficiently large to predict the left-out subjects' MRS-GABA with performance above chance. We repeated the analysis this time with the only NMM-phasic parameter which showed a significant relationship with GABA, namely the inhibitory connection from the inhibitory interneurons to the deep pyramidal cells (NMM-II-DP connection). The LOO was not significant (Pearsons's rho $= -0.03$, $P = 0.55$), thus revealing that MRS-GABA cannot be predicted by the II-DP connection (Fig. 5*E*). We further tested whether the percentage of menstrual cycle could account for the associations in Fig. 5*D* and *E*. The analysis was performed again on the NMM-self_II and the NMM-II-DP connection. One participant was excluded due to contraceptive use, leaving a final sample of 19 participants. The findings remain unchanged: even after accounting for menstrual cycle phase, MRS-GABA continues to be significantly predicted by the NMM-self_II parameter (Fig. 5*F*) but not by the II-DP connection (Fig. 5*G*).

Discussion

MRS enables non-invasive *in vivo* measurements of neurotransmitter concentration in the brain. Despite the increasing number of MRS-based findings on the role of GABA in human behaviour, learning, and neurological disorders, their relevance in terms of cortical network dynamics remains uncertain. This uncertainty limits the interpretation of MRS results, especially when one wants to relate MRS-GABA to behaviour or pathological processes.

Here we collected 7 T MRS and TMS-EEG data over M1 in 20 young healthy participants. We then applied a biophysical NMM on our electrophysiological data to establish potential relationships between modelled neurophysiological parameters and MRS. We show that MRS-GABA was closely related to tonic inhibition, being positively associated with the interneurons, stellate cells and deep pyramidal cells' (tonic) inhibitory feedback loops. MRS-GABA was also associated with the functioning of the GABAergic synapse at large, as indexed by the $GABA_A$ parameter, which mediates all (tonic and phasic) inhibitory connections allowed in
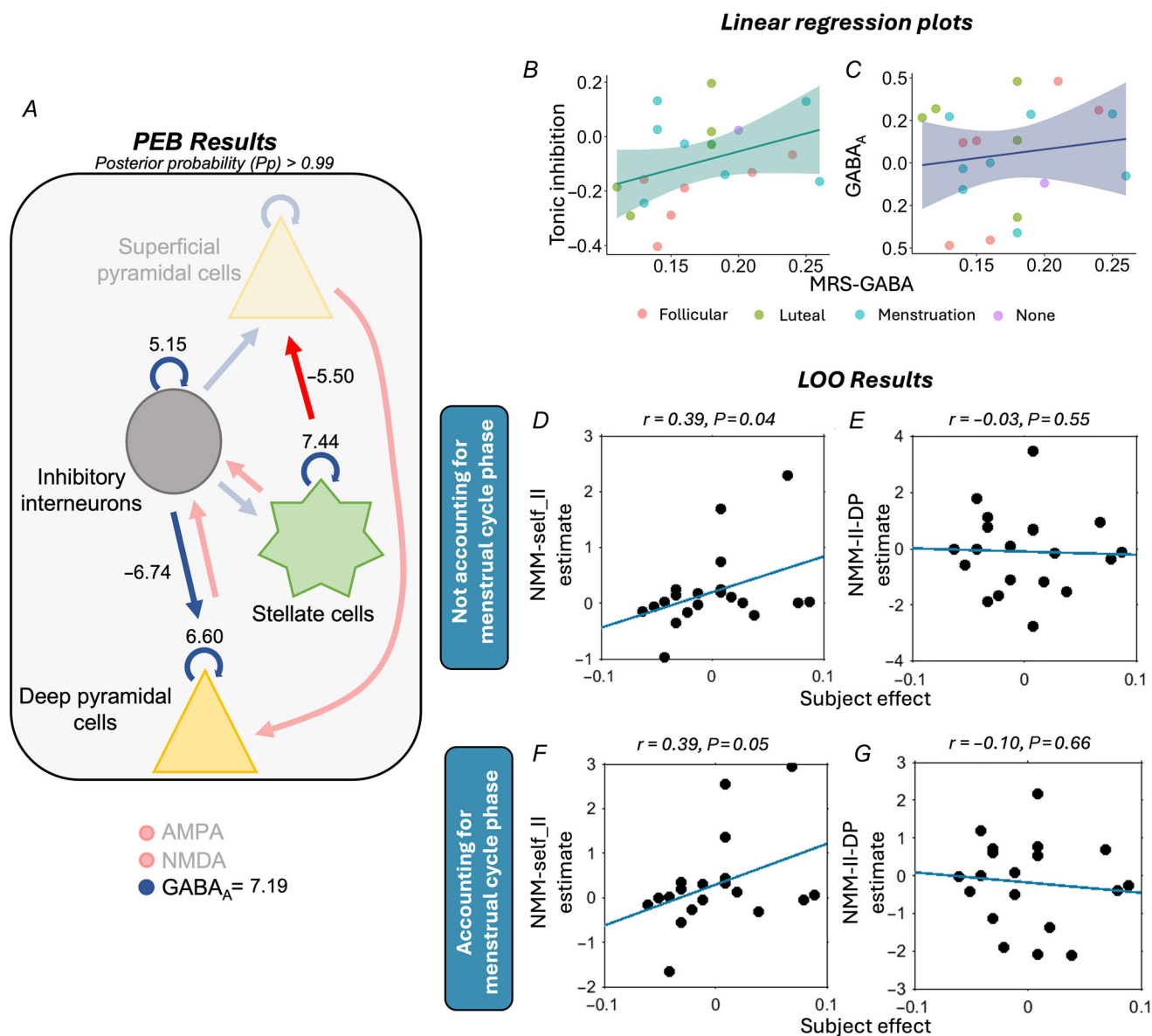
Figure 5. Association between NMM parameters and MRS GABA
A, outcomes of the PEB analyses. Only parameters showing a significant relationship with MRS-GABA (Pp > 0.99) are highlighted. The sign indicates the direction of the relationship (positive or negative) whereas the values indicate the rate of change of each parameter as a function of MRS-GABA. Overall, we observed that MRS-GABA was positively related to the tonic inhibition of the inhibitory interneurons, stellate cells and deep pyramidal cells, whereas it was negatively related to the excitatory connection from stellate to superficial pyramidal cells and to the inhibitory connection from inhibitory interneurons to deep pyramidal cells. Among the receptors, MRS-GABA was shown to be only positively related to the activity of GABA$_A$. *B* and *C*, regression plots representing the positive effects found between MRS-GABA and the NMM-derived GABAergic measures: tonic inhibition, calculated as the mean of the significant self-inhibitory feedback loop peak estimates (*B*) and the activity of the GABA$_A$ receptor (*C*). These plots are for display purposes only and do not substitute the outcomes of the PEB analysis. Menstrual cycle phase was also represented by colour-coding data points according to cycle phase categories. *D–G*, LOO analyses accounting or not for hormonal phase. The actual subject effect is plotted against the expected value of the estimated subject effect. This analysis allows us to test whether the relationship found between NMM-self_II/ NMM-II-DP and MRS-GABA is meaningful enough that one could predict one based on the other. For the NMM-self_II, we found a significant relationship between the actual MRS-GABA and the predicted MRS-GABA for each left-out subject (Pearsons's rho = 0.39, *P* = 0.04) (*D*), even when hormonal phase was accounted for (Pearsons's rho = 0.39, *P* = 0.05) (*F*). That was not the case when we tested the NMM-II-DP connection (Pearsons's rho = −0.03, *P* = 0.55) (*E*), even when accounting for the hormonal phase (Pearsons's rho = −0.10, *P* = 0.66) (*G*).

the model. The relationship observed between MRS- and tonic NMM-GABA was meaningful enough that we could predict the left-out subjects' MRS-GABA from the NMM-GABA, taking as a proxy of NMM-tonic inhibition the activity of the inhibitory interneurons' feedback loop. Importantly, that was not the case when the same analysis was repeated with the only NMM-phasic inhibition parameter showing a significant effect with MRS-GABA, namely the inhibitory connection from the inhibitory interneurons to the deep pyramidal cells. Results were confirmed even when accounting for participants' hormonal phase.

NMM helps clarify what is being measured by MRS-GABA

The morphology of the motor cortex (Georgopoulos & Stefanis, 2007; Somogyi et al., 1998) is now well established. The majority of neurons are pyramidal cells, although 28% are interneurons, of which the majority are excitatory or spiny stellate cells (Sloper & Powell, 1979). Stellate cells are mostly found in layer 4 of the cortex (Schubert et al., 2003), and for many years it was thought that the motor cortex did not have a layer IV, suggesting that the neural circuitry controlling motor movements was different from other cortical regions. However, multiple lines of evidence have challenged this view by showing that neurons at the border between layer 3 and 5 of the motor cortex possess many of the same proprieties of stellate cells (Yamawaki et al., 2014) and are distributed in several layers, even in more superficial ones (Porter et al., 1990). The convoluted and fine-tuned connections between pyramidal cells and interneurons are used to adjust the balance between excitation and inhibition and finely select the output of the circuit (di Lazzaro et al., 2016).

To best capture the functioning of a cortical motor network, the NMM used in this study comprised all three above-mentioned cell types with the pyramidal cells further subdivided into superficial and deep. The resulting four subpopulations of neurons, whose activity is controlled and regulated by self-inhibitory feedback loops, form excitatory or inhibitory connections mediated by AMPA and NMDA or $GABA_A$ receptors, respectively. TMS is thought to enter this network by inducing a strong depolarization of the superficial pyramidal cells (di Lazzaro & Ziemann, 2013), which, in turn, leads to the recruitment of fully synchronized clusters of deep pyramidal neurons and interneurons to control the firing of excitatory networks and adjust the excitation/inhibition balance (di Lazzaro et al., 2016). To further describe the complex cortical circuitry, our NMM distinguishes between inhibitory self-connections and inhibitory projections from interneurons to the other cells. Self-connections are assumed to mediate tonic back-

ground inhibition, while intrinsic inputs to pyramidal and stellate cells can be regarded as mediating phasic inhibition (Adams et al., 2021a).

When using PEB analysis to reveal potential associations between MRS-GABA and NMM parameters we observed that MRS-GABA was positively related to the self-inhibitory feedback loops (i.e. tonic inhibition) of almost all neural subpopulations, except the superficial pyramidal cells, which were most probably receiving the TMS input. Higher MRS-GABA was associated with higher tonic inhibition of deep pyramidal cells, stellate cells and inhibitory interneurons. Consequently, more inhibited stellate cells excited less superficial pyramidal cells whereas more inhibited interneurons inhibited less deep pyramidal cells. The analysis also revealed a positive relationship between MRS-GABA and $GABA_A$ receptor activity, which is a time constant that encodes how fast inhibitory post-synaptic potentials recover after a pre-synaptic spike has reached the dendrite, thus reflecting the functioning of the inhibitory synapse at large.

Our findings align with several other studies that tried to relate MRS-GABA to measures of phasic inhibition in humans and found no significant relationships. Phasic inhibition was either assessed through TMS using paired pulses with different interstimulus intervals (Dyke et al., 2017; Mooney et al., 2017; Stagg, Bestmann, et al., 2011; Tremblay et al., 2013), or through [^{11}C]flumazenil PET, a radiotracer that binds to the benzodiazepine site of $GABA_A$ receptors thus providing a more direct quantification of the receptors availability at the level of the synapse (Cuypers et al., 2021). MRS-GABA showed only one significant relationship with what is believed to be a paired-pulse TMS measure of tonic inhibition (Stagg, 2014; Stagg, Bestmann, et al., 2011), even though this result has not been replicated in more recent studies (Dyke et al., 2017; Mooney et al., 2017). By showing that MRS-GABA mostly relates to parameters that code for tonic inhibition in a biophysical NMM, our study confirms empirically what a recent mathematical simulation seemed to suggest (Lea-Carnall et al., 2023), and may further explain why the previous attempts to relate MRS-GABA to measures of phasic inhibition failed.

Our study does not come without flaws. First, the sample size is relatively small. A larger sample size would have increased statistical power, though relationships with meaningful effect sizes should be evident with this sample size. Second, our sample comprised young females only, limiting the generalizability of the findings. Third, technical constraints make it impossible to obtain a perfect overlap between MRS voxel and TMS-EEG motor hotspot. The MRS voxel was placed as close as possible to the TMS-EEG motor hotspot, which is, however, fairly superficial. Thus, a complete overlap between the MRS voxel and the TMS spot would have resulted in the MRS voxel crossing the dura, thus compromising spectral quality by

introducing lipid artifacts. The choice of not to rotate the voxel further was made to ensure good spectral quality, as excessive rotations of the voxel (>45°) may change the ordering of the gradients and the amount of artifact in the spectra. Finally, and most obviously, NMM does not provide a direct measure of the actual biological process but a validated approximation. Invasive electrophysiological measurements in pathological brains of patients undergoing surgery could partly address this limitation although interneurons are more difficult to record using multiunit recordings. Future studies could also assess MRS-GABA before and after pharmacological manipulation of ambient/tonic GABA. Likewise, animal models could combine ultra-high-field MRS at 9.4 T (Nassirpour et al., 2018) and opto- and chemogenetics to further validate the mechanistic links between MRS signal and GABAergic neurotransmission (Takado et al., 2022).

The importance of elucidating GABAergic measures in the clinical context

GABAergic inhibition has a major impact on information processing, plasticity and network synchronization (Bhat et al., 2010), and its clinical relevance in many neurological disorders has been proven. Epilepsy is an obvious example. Changes in inhibitory neurotransmissions are found in both animal models (Bouilleret et al., 2000) and human epileptic patients (Olsen, 1997). Epileptogenic phenomena have been associated with episodes of excitatory or inhibitory cellular hyperactivity, changes in traffic and expression of GABA receptors, and disequilibrium between tonic inhibition and neuronal excitability in animals (van van Hugte et al., 2023). In humans, studies testing GABAergic changes in epilepsy showed increased GABA levels in patients with juvenile myoclonic epilepsy (Hattingen et al., 2014), idiopathic generalized epilepsy (Chowdhury et al., 2015) and refractory focal epilepsy (Simister et al., 2007), which were associated with malformations of cortical development compared to controls.

Beyond epilepsy, stroke represents another clinical example of disruption and imbalance between excitatory and inhibitory activity in the brain. Studies investigating GABAergic alterations following stroke revealed a lower GABA concentration in the contralesional M1 (Cirillo et al., 2020), decreased GABA concentration following constraint-induced motor therapy (Blicher et al., 2015) and lower $GABA_A$ receptor activity in the ipsilesional M1 (Swayne et al., 2008), causing an overall higher excitation/inhibition ratio in the affected hemisphere (McDonnell & Stinear, 2017), which was inversely correlated with motor recovery (Talelli et al., 2006).

GABAergic changes have been highlighted in other neurological and psychiatric disorders, such

as relapsing–remitting multiple sclerosis (Cao et al., 2018), Alzheimer's disease (Jiménez-Balado & Eich, 2021) and Parkinson's disease (Song et al., 2021), substance use disorder (Shyu et al., 2022), schizophrenia (Kumar et al., 2021) and autism spectrum disorder (Maier et al., 2022), to name a few. Most of the studies use MRS to quickly and non-invasively quantify GABA in patients. Knowing that these GABAergic alterations found in patients *versus* controls do not apply to any type of GABA but specifically to tonic GABA may inform novel interventions and therapeutic targets to ensure more tailored treatments. The development of drugs able to alter tonic GABA by acting on extrasynaptic GABA receptors has seen remarkable progress. For instance, GABAmimetic drugs, such as muscimol and THIP (gaboxadol; 4,5,6,7-tetrahydroisoxazolol[4,5-c]pyridine-3-ol), have been shown to act on $GABA_A$ receptor agonist sites with preferential activation of the high-affinity extrasynaptic receptors (Chandra et al., 2010).

Conclusions

MRS is increasingly being used to investigate GABAergic changes in inter-individual behavioural differences and in the context of neurological disorders. Recent advances in MRS, such as high-resolution 3-D imaging of metabolic profiles over large brain regions by MRS imaging at ultra-high field (Lemke et al., 2015), increase the promise of MRS as a clinical tool. Our study provides empirical data to clarify the mesoscopic underpinnings of MRS-GABA, supporting the idea that it primarily measures extrasynaptic GABA activity (i.e. tonic inhibition). Elucidating its functional significance will improve our understanding of human behaviour, brain physiology and pathophysiology.

References

Adams, N. E., Hughes, L. E., Rouse, M. A., Phillips, H. N., Shaw, A. D., Murley, A. G., Cope, T. E., Bevan-Jones, W. R., Passamonti, L., Street, D., Holland, N., Nesbitt, D., Friston, K., & Rowe, J. B. (2021a). GABAergic cortical network physiology in frontotemporal lobar degeneration. *Brain*, **144**(7), 2135–2145.

Adams, N. E., Hughes, L. E., Rouse, M. A., Phillips, H. N., Shaw, A. D., Murley, A. G., Cope, T. E., Bevan-Jones, W. R., Passamonti, L., Street, D., Holland, N., Nesbitt, D., Friston, K., & Rowe, J. B. (2021b). GABAergic cortical network physiology in frontotemporal lobar degeneration. *Brain*, **144**(7), 2135–2145.

Bachtiar, V., Near, J., Johansen-Berg, H., & Stagg, C. J. (2015). Modulation of GABA and resting state functional connectivity by transcranial direct current stimulation. *eLife*, **4**, 1–9.

Belelli, D., Harrison, N. L., Maguire, J., Macdonald, R. L., Walker, M. C., & Cope, D. W. (2009). Extrasynaptic GABAA receptors: Form, pharmacology, and function. *Journal of Neuroscience*, **29**(41), 12757–12763.

Bhat, R., Axtell, R., Mitra, A., Miranda, M., Lock, C., Tsien, R. W., & Steinman, L. (2010). Inhibitory role for GABA in autoimmune inflammation. *Proceedings of the National Academy of Sciences*, **107**(6), 2580–2585.

Blicher, J. U., Near, J., Næss-Schmidt, E., Stagg, C. J., Johansen-Berg, H., Nielsen, J. F., Østergaard, L., & Ho, Y.-C. L. (2015). GABA levels are decreased after stroke and GABA changes during rehabilitation correlate with motor improvement. *Neurorehabilitation and Neural Repair*, **29**(3), 278–286.

Bouilleret, V., Loup, F., Kiener, T., Marescaux, C., & Fritschy, J. (2000). Early loss of interneurons and delayed subunit-specific changes in GABAA-receptor expression in a mouse model of mesial temporal lobe epilepsy. *Hippocampus*, **10**(3), 305–324.

Cao, G., Edden, R. A. E., Gao, F., Li, H., Gong, T., Chen, W., Liu, X., Wang, G., & Zhao, B. (2018). Reduced GABA levels correlate with cognitive impairment in patients with relapsing-remitting multiple sclerosis. *European Radiology*, **28**(3), 1140–1148.

Chandra, D., Halonen, L. M., Linden, A.-M., Procaccini, C., Hellsten, K., Homanics, G. E., & Korpi, E. R. (2010). Prototypic GABAA receptor agonist muscimol acts preferentially through forebrain high-affinity binding sites. *Neuropsychopharmacology*, **35**(4), 999–1007.

Chang, L., Jiang, C. S., & Ernst, T. (2009). Effects of age and sex on brain glutamate and other metabolites. *Magnetic Resonance Imaging*, **27**(1), 142–145.

Chellappa, S. L., Gaggioni, G., Ly, J. Q. M., Papachilleos, S., Borsu, C., Brzozowski, A., Rosanova, M., Sarasso, S., Luxen, A., Middleton, B., Archer, S. N., Dijk, D. J., Massimini, M., Maquet, P., Phillips, C., Moran, R. J., & Vandewalle, G. (2016). Circadian dynamics in measures of cortical excitation and inhibition balance. *Scientific Reports*, **6**, 1–13.

Chowdhury, F. A., O'Gorman, R. L., Nashef, L., Elwes, R. D., Edden, R. A., Murdoch, J. B., Barker, G. J., & Richardson, M. P. (2015). Investigation of glutamine and GABA levels in patients with idiopathic generalized epilepsy using MEGAPRESS. *Journal of Magnetic Resonance Imaging*, **41**(3), 694–699.

Cirillo, J., Mooney, R. A., Ackerley, S. J., Barber P. A., Borges, V. M., Clarkson, A. N., Mangold, C., Ren, A., Smith, M. C., Stinear, C. M., & Byblow, W. D. (2020). Neurochemical balance and inhibition at the subacute stage after stroke. *Journal of Neurophysiology*, **123**(5), 1775–1790.

Clarke, W. T., Bell, T. K., Emir, U. E., Mikkelsen, M., Oeltzschner, G., Shamaei, A., Soher, B. J., & Wilson, M. (2022). NIfTI-MRS: A standard data format for magnetic resonance spectroscopy. *Magnetic Resonance in Medicine*, **88**(6), 2358–2370.

Clarke, W. T., Stagg, C. J., & Jbabdi, S. (2021). FSL-MRS: An end-to-end spectroscopy analysis package. *Magnetic Resonance in Medicine*, **85**(6), 2950–2964.

Cuypers, K., Hehl, M., van Aalst, J., Chalavi, S., Mikkelsen, M., Van Laere, K., Dupont, P., Mantini, D., & Swinnen, S. P. (2021). Age-related GABAergic differences in the primary sensorimotor cortex: A multimodal approach combining PET, MRS and TMS. *Neuroimage*, **226**, 117536.

Di Lazzaro, V., Capone, F., Paolucci, M., Assenza, F., Brunelli, N., Ricci, L., & Florio, L. (2016). Canonical cortical circuits: Current evidence and theoretical implications. *Neuroscience and Neuroeconomics*, **2016**, 1.

di Lazzaro, V., & Ziemann, U. (2013). The contribution of transcranial magnetic stimulation in the functional evaluation of microcircuits in human motor cortex. *Frontiers in Neural Circuits*, **7**, 18.

Dyke, K., Pépés, S. E., Chen, C., Kim, S., Sigurdsson, H. P., Draper, A., Husain, M., Nachev, P., Gowland, P. A., & Morris, P. G. (2017). Comparing GABA-dependent physiological measures of inhibition with proton magnetic resonance spectroscopy measurement of GABA using ultra-high-field MRI. *Neuroimage*, **152**, 360–370.

Epperson, C. N., Haga, K., Mason, G. F., Sellers, E., Gueorguieva, R., Zhang, W., Weiss, E., Rothman, D. L., & Krystal, J. H. (2002). Cortical γ-aminobutyric acid levels across the menstrual cycle in healthy women and those with premenstrual dysphoric disorder: A proton magnetic resonance spectroscopy study. *Archives of General Psychiatry*, **59**(9), 851–858.

Erdfelder, E., FAul, F., Buchner, A., & Lang, A. G. (2009). Statistical power analyses using G*Power 3.1: Tests for correlation and regression analyses. *Behavior Research Methods*, **41**(4), 1149–1160.

Fecchio, M., Pigorini, A., Comanducci, A., Sarasso, S., Casarotto, S., Premoli, I., Derchi, C.-C., Mazza, A., Russo, S., & Resta, F. (2017). The spectral features of EEG responses to transcranial magnetic stimulation of the primary motor cortex depend on the amplitude of the motor evoked potentials. *PLoS ONE*, **12**(9), e0184910.

Friston, K. J., Harrison, L., & Penny, W. (2003). Dynamic causal modelling. *Neuroimage*, **19**(4), 1273–1302.

Georgopoulos, A. P., & Stefanis, C. N. (2007). Local shaping of function in the motor cortex: Motor contrast, directional tuning. *Brain Research Reviews*, **55**(2 SPEC. ISS.), 383–389.

Gilfarb, R. A., & Leuner, B. (2022). GABA system modifications during periods of hormonal flux across the female lifespan. *Frontiers in Behavioral Neuroscience*, **16**, 802530.

Gruetter, R., & Tkáč, I. (2000). Field mapping without reference scan using asymmetric echo-planar techniques. *Magnetic Resonance in Medicine: An Official Journal of the International Society for Magnetic Resonance in Medicine*, **43**(2), 319–323.

Hattingen, E., Lückerath, C., Pellikan, S., Vronski, D., Roth, C., Knake, S., Kieslich, M., & Pilatus, U. (2014). Frontal and thalamic changes of GABA concentration indicate dysfunction of thalamofrontal networks in juvenile myoclonic epilepsy. *Epilepsia*, **55**(7), 1030–1037.

Hernandez-Pavon, J. C., Veniero, D., Bergmann, T. O., Belardinelli, P., Bortoletto, M., Casarotto, S., Casula, E. P., Farzan, F., Fecchio, M., Julkunen, P., Kallioniemi, E., Lioumis, P., Metsomaa, J., Miniussi, C., Mutanen, T. P., Rocchi, L., Rogasch, N. C., Shafi, M. M., Siebner, H. R., … Ilmoniemi, R. J. (2023). TMS combined with EEG: Recommendations and open issues for data collection and analysis. *Brain Stimulation*, **16**(2), 567–593.

Jenkinson, M., Beckmann, C. F., Behrens, T. E. J., Woolrich, M. W., & Smith, S. M. (2012). Fsl. *Neuroimage*, **62**(2), 782–790.

Jenkinson, M., & Smith, S. (2001). A global optimisation method for robust affine registration of brain images. *Medical Image Analysis*, **5**(2), 143–156.

Jiménez-Balado, J., & Eich, T. S. (2021). GABAergic dysfunction, neural network hyperactivity and memory impairments in human aging and Alzheimer's disease. *Seminars in Cell & Developmental Biology*, **116**, 146–159.

Juchem, C., Cudalbu, C., de Graaf, R. A., Gruetter, R., Henning, A., Hetherington, H. P., & Boer, V. O. (2021). B0 shimming for in vivo magnetic resonance spectroscopy: Experts' consensus recommendations. *Nuclear Magnetic Resonance in Biomedicine*, **34**(5), 1–20.

Kolasinski, J., Hinson, E. L., Divanbeighi Zand, A. P., Rizov, A., Emir, U. E., & Stagg, C. J. (2019). The dynamics of cortical GABA in human motor learning. *The Journal of Physiology*, **597**(1), 271–282.

Kumar, V., Vajawat, B., & Rao, N. P. (2021). Frontal GABA in schizophrenia: A meta-analysis of 1H-MRS studies. *The World Journal of Biological Psychiatry*, **22**(1), 1–13.

Le Roux, N., Amar, M., Moreau, A., Baux, G., & Fossier, P. (2008). Impaired GABAergic transmission disrupts normal homeostatic plasticity in rat cortical networks. *European Journal of Neuroscience*, **27**(12), 3244–3256.

Lea-Carnall, C. A., El-Deredy, W., Stagg, C. J., Williams, S. R., & Trujillo-Barreto, N. J. (2023). A mean-field model of glutamate and GABA synaptic dynamics for functional MRS. *Neuroimage*, **266**, 119813.

Lemke, C., Hess, A., Clare, S., Bachtiar, V., Stagg, C., Jezzard, P., & Emir, U. (2015). Two-voxel spectroscopy with dynamic B0 shimming and flip angle adjustment at 7 T in the human motor cortex. *Nuclear Magnetic Resonance in Biomedicine*, **28**(7), 852–860.

Lin, A., Andronesi, O., Bogner, W., Choi, I., Coello, E., Cudalbu, C., Juchem, C., Kemp, G. J., Kreis, R., & Krššák, M. (2021). Minimum reporting standards for in vivo magnetic resonance spectroscopy (MRSinMRS): Experts' consensus recommendations. *Nuclear Magnetic Resonance in Biomedicine*, **34**(5), e4484.

Maguire, J. L., Stell, B. M., Rafizadeh, M., & Mody, I. (2005). Ovarian cycle–linked changes in GABAA receptors mediating tonic inhibition alter seizure susceptibility and anxiety. *Nature Neuroscience*, **8**(6), 797–804.

Maier, S., Düppers, A. L., Runge, K., Dacko, M., Lange, T., Fangmeier, T., Riedel, A., Ebert, D., Endres, D., & Domschke, K. (2022). Increased prefrontal GABA concentrations in adults with autism spectrum disorders. *Autism Research*, **15**(7), 1222–1236.

McDonnell, M. N., & Stinear, C. M. (2017). TMS measures of motor cortex function after stroke: A meta-analysis. *Brain Stimulation*, **10**(4), 721–734.

Mooney, R. A., Cirillo, J., & Byblow, W. D. (2017). GABA and primary motor cortex inhibition in young and older adults: A multimodal reliability study. *Journal of Neurophysiology*, **118**(1), 425–433.

Moran, R. J., Jung, F., Kumagai, T., Endepols, H., Graf, R., Dolan, R. J., Friston, K. J., Stephan, K. E., & Tittgemeyer, M. (2011). Dynamic causal models and physiological inference: A validation study using isoflurane anaesthesia in rodents. *PLoS ONE*, **6**(8), e22790.

Moran, R. J., Kiebel, S. J., Stephan, K. E., Reilly, R. B., Daunizeau, J., & Friston, K. J. (2007). A neural mass model of spectral responses in electrophysiology. *Neuroimage*, **37**(3), 706–720.

Moran, R. J., Pinotsis, D. A., & Friston, K. J. (2013). Neural masses and fields in dynamic causal modeling. *Frontiers in Computational Neuroscience*, **7**, 57.

Moran, R. J., Symmonds, M., Stephan, K. E., Friston, K. J., & Dolan, R. J. (2011). An in vivo assay of synaptic function mediating human cognition. *Current Biology*, **21**(15), 1320–1325.

Mullins, P. G., McGonigle, D. J., O'Gorman, R. L., Puts, N. A. J., Vidyasagar, R., Evans, C. J., & Edden, R. A. E. (2014). Current practice in the use of MEGA-PRESS spectroscopy for the detection of GABA. *Neuroimage*, **86**, 43–52.

Muthukumaraswamy, S. D., Carhart-Harris, R. L., Moran, R. J., Brookes, M. J., Williams, T. M., Errtizoe, D., Sessa, B., Papadopoulos, A., Bolstridge, M., Singh, K. D., Feilding, A., Friston, K. J., & Nutt, D. J. (2013). Broadband cortical desynchronization underlies the human psychedelic state. *Journal of Neuroscience*, **33**(38), 15171–15183.

Muthukumaraswamy, S. D., Shaw, A. D., Jackson, L. E., Hall, J., Moran, R., & Saxena, N. (2015). Evidence that sub-anesthetic doses of ketamine cause sustained disruptions of NMDA and AMPA-mediated frontoparietal connectivity in humans. *Journal of Neuroscience*, **35**(33), 11694–11706.

Nassirpour, S., Chang, P., & Henning, A. (2018). High and ultra-high resolution metabolite mapping of the human brain using ^{1}H FID MRSI at 9.4T. *NeuroImage*, **168**, 211–221.

Near, J., Harris, A. D., Juchem, C., Kreis, R., Marjańska, M., Öz, G., Slotboom, J., Wilson, M., & Gasparovic, C. (2021). Preprocessing, analysis and quantification in single-voxel magnetic resonance spectroscopy: Experts' consensus recommendations. *Nuclear Magnetic Resonance in Biomedicine*, **34**(5), 1–23.

O'Gorman, R. L., Michels, L., Edden, R. A., Murdoch, J. B., & Martin, E. (2011). In vivo detection of GABA and glutamate with MEGA-PRESS: Reproducibility and gender effects. *Journal of Magnetic Resonance Imaging*, **33**(5), 1262–1267.

Olsen, R. W. (1997). GABA receptor function and epilepsy. *Basic Mechanisms of the Epilepsies*.

Pandya, M., Palpagama, T. H., Turner, C., Waldvogel, H. J., Faull, R. L., & Kwakowsky, A. (2019). Sex- and age-related changes in GABA signaling components in the human cortex. *Biology of Sex Differences*, **10**(1), 1–16.

Paparella, I., Vandewalle, G., Stagg, C. J., & Maquet, P. (2023). An integrated measure of GABA to characterize post-stroke plasticity. *NeuroImage: Clinical*, **39**, 103463.

Parrott, A. C., & Hindmarch, I. (1978). Factor analysis of a sleep evaluation questionnaire. *Psychological Medicine*, **8**(2), 325–329.

Porter, L. L., Sakamoto, T., & Asanuma, H. (1990). Morphological and physiological identification of neurons in the cat motor cortex which receive direct input from the somatic sensory cortex. *Experimental Brain Research*, **80**(1), 209–212.

Sanacora, G., Mason, G. F., Rothman, D. L., Behar, K. L., Hyder, F., Petroff, O. A. C., Berman, R. M., Charney, D. S., & Krystal, J. H. (1999). Reduced cortical γ-aminobutyric acid levels in depressed patients determined by proton magnetic resonance spectroscopy. *Archives of General Psychiatry*, **56**(11), 1043–1047.

Schubert, D., Kötter, R., Zilles, K., Luhmann, H. J., & Staiger, J. F. (2003). Cell type-specific circuits of cortical layer IV spiny neurons. *Journal of Neuroscience*, **23**(7), 2961–2970.

Shyu, C., Chavez, S., Boileau, I., & Le Foll, B. (2022). Quantifying GABA in addiction: A review of proton magnetic resonance spectroscopy studies. *Brain Sciences*, **12**(7), 918.

Simister, R. J., McLean, M. A., Barker, G. J., & Duncan, J. S. (2007). Proton magnetic resonance spectroscopy of malformations of cortical development causing epilepsy. *Epilepsy Research*, **74**(2–3), 107–115.

Sloper, J. J., & Powell, T. P. S. (1979). An experimental electron microscopy study of afferent connections to the primate motor and somatic sensory cortices. *Philosophical Transactions of the Royal Society of London B, Biological Sciences*, **285**(1006), 199–226.

Smith, S. M. (2002). Fast robust automated brain extraction. *Human Brain Mapping*, **17**(3), 143–155.

Somogyi, P., Tamas, G., Lujan, R., & Buhl, E. H. (1998). Salient features of synaptic organisation in the cerebral cortex. *Brain Research Reviews*, **26**(2–3), 113–135.

Song, Y., Gong, T., Saleh, M. G., Mikkelsen, M., Wang, G., & Edden, R. A. E. (2021). Upper brainstem GABA levels in Parkinson's disease. *Magnetic Resonance Materials in Physics, Biology and Medicine*, **34**(5), 689–696.

Stagg, C. J. (2014). Magnetic resonance spectroscopy as a tool to study the role of GABA in motor-cortical plasticity. *Neuroimage*, **86**, 19–27.

Stagg, C. J., Bachtiar, V., Amadi, U., Gudberg, C. A., Ilie, A. S., Sampaio-Baptista, C., O'Shea, J., Woolrich, M., Smith, S. M., Filippini, N., Near, J., & Johansen-Berg, H. (2014). Local GABA concentration is related to network-level resting functional connectivity. *eLife*, **2014**(3), 1–9.

Stagg, C. J., Bachtiar, V., & Johansen-Berg, H. (2011a). The role of GABA in human motor learning. *Current Biology*, **21**(6), 480–484.

Stagg, C. J., Bachtiar, V., & Johansen-Berg, H. (2011b). What are we measuring with GABA Magnetic resonance spectroscopy? *Communicative & Integrative Biology*, **4**(5), 573–575.

Stagg, C. J., Bestmann, S., Constantinescu, A. O., Moreno Moreno, L., Allman, C., Mekle, R., Woolrich, M., Near, J., Johansen-Berg, H., & Rothwell, J. C. (2011). Relationship between physiological measures of excitability and levels of glutamate and GABA in the human motor cortex. *The Journal of Physiology*, **589**(23), 5845–5855.

Swayne, O. B. C., Rothwell, J. C., Ward, N. S., & Greenwood, R. J. (2008). Stages of motor output reorganization after hemispheric stroke suggested by longitudinal studies of cortical physiology. *Cerebral Cortex*, **18**(8), 1909–1922.

Takado, Y., Takuwa, H., Sampei, K., Urushihata, T., Takahashi, M., Shimojo, M., Uchida, S., Nitta, N., Shibata, S., Nagashima, K., Ochi, Y., Ono, M., Maeda, J., Tomita, Y., Sahara, N., Near, J., Aoki, I., Shibata, K., & Higuchi, M. (2022). MRS-measured glutamate versus GABA reflects excitatory versus inhibitory neural activities in awake mice. *Journal of Cerebral Blood Flow and Metabolism*, **42**(1), 197–212.

Talelli, P., Greenwood, R. J., & Rothwell, J. C. (2006). Arm function after stroke: Neurophysiological correlates and recovery mechanisms assessed by transcranial magnetic stimulation. *Clinical Neurophysiology*, **117**(8), 1641–1659.

Tremblay, S., Beaulé, V., Proulx, S., De Beaumont, L., Marjańska, M., Doyon, J., Pascual-Leone, A., Lassonde, M., & Théoret, H. (2013). Relationship between transcranial magnetic stimulation measures of intracortical inhibition and spectroscopy measures of GABA and glutamate+glutamine. *Journal of Neurophysiology*, **109**(5), 1343–1349.

van van Hugte, E. J. H., Schubert, D., & Nadif Kasri, N. (2023). Excitatory/inhibitory balance in epilepsies and neuro-developmental disorders: Depolarizing γ-aminobutyric acid as a common mechanism. *Epilepsia*, **64**(8), 1975–1990.

Yamawaki, N., Borges, K., Suter, B. A., Harris, K. D., & Shepherd, G. M. G. (2014). A genuine layer 4 in motor cortex with prototypical synaptic circuit connectivity. *eLife*, **3**, e05422.

Zeidman, P., Jafarian, A., Corbin, N., Seghier, M. L., Razi, A., Price, C. J., & Friston, K. J. (2019). A guide to group effective connectivity analysis, part 1: First level analysis with DCM for fMRI. *Neuroimage*, **200**, 174–190.

Zeidman, P., Jafarian, A., Seghier, M. L., Litvak, V., Cagnan, H., Price, C. J., & Friston, K. J. (2019). A guide to group effective connectivity analysis, part 2: Second level analysis with PEB. *Neuroimage*, **200**, 12–25.

Zhang, W., Xiong, B.-R., Zhang, L.-Q., Huang, X., Yuan, X., Tian, Y.-K., & Tian, X.-B. (2021). The role of the GABAergic system in diseases of the central nervous system. *Neuroscience*, **470**, 88–99.

Zhang, Y., Brady, M., & Smith, S. (2001). Segmentation of brain MR images through a hidden Markov random field model and the expectation-maximization algorithm. *Institute of Electrical and Electronics Engineers Transactions on Medical Imaging*, **20**(1), 45–57.

Additional information

Data availability statement

The processed data and analysis scripts supporting the results included in this paper are publicly available via the following open repository: https://gitlab.uliege.be/CyclotronResearchCentre/Public/fasst/mrs-gaba-nmm. The raw MRI data could be identified and linked to a single subject and represent a large amount of data. Researchers wishing to access to the raw should send a request to the

senior corresponding author (G.V.). Data sharing will require evaluation of the request by the local Research Ethics Board and the signature of a data transfer agreement (DTA).

Competing interests

The authors declare that they have no competing interests.

Author contributions

I.P., G.V. and P.M. designed the research. I.P. and P.C. set up the experiment. I.P., P.C. and B.Z. acquired the data. C.J.S., W.C. and S.S. supported data acquisition by providing MRS sequences. L.L., F.C. and M.Z. gave important insights while discussing and interpreting the data. I.P. analysed the data supervised by G.V. regarding the TMS-EEG part, and by W.C. and C.J.S. for the MRS part. I.P., P.M. and G.V. wrote the paper. All authors edited and approved the final version of the manuscript.

Funding

Acknowledgements

Keywords

GABA, inhibition, magnetic resonance spectroscopy (MRS), motor cortex, neural mass model, TMS-EEG

Supporting information

Additional supporting information can be found online in the Supporting Information section at the end of the HTML view of the article. Supporting information files available:

Peer Review History

Translational perspective

GABAergic inhibition has a major impact on human information processing, plasticity and network synchronization, and its clinical relevance in many neurological disorders, including stroke, epilepsy and multiple sclerosis, has been proven. Quantification of bulk GABA in the human brain is typically obtained by magnetic resonance spectroscopy (MRS). However, which GABAergic pool is being measured by MRS is still debated. Here we collected ultra-high-field 7 T MRS and transcranial magnetic stimulation coupled with high-density electroencephalography (TMS-hdEEG) from the motor cortex of 20 healthy female participants (age 23.95 ± 6.4 years), while they were at rest. Through the application of a mathematical model to TMS-evoked potentials to disentangle the contribution of different GABAergic pools, we found that MRS-GABA was mostly positively related to the model-derived measures of tonic inhibition. This relationship was reliable enough to have predictive value. Our findings help clarifying the mesoscopic underpinnings of GABA levels measured with MRS by supporting the idea that it primarily measures extrasynaptic GABA activity (i.e. tonic inhibition). Elucidating MRS-GABA functional significance will improve our understanding of human behaviour, brain physiology and pathophysiology. Indeed, as MRS is often used to quickly and non-invasively quantify GABA in patients, knowing that GABAergic alterations reported in several clinical populations *versus* controls do not apply to any type of GABA but specifically to tonic GABA may inform novel interventions and therapeutic targets to ensure more tailored treatments, such as push for a development of drugs able to alter tonic GABA by acting on extrasynaptic GABA receptors.